infrastructures

MDPI

Article

Assessment and Fragility of Byzantine Unreinforced Masonry Towers

Emmanouil-Georgios Kouris [1], Leonidas-Alexandros S. Kouris [1,*], Avraam A. Konstantinidis [1], Chris G. Karayannis [2] and Elias C. Aifantis [1]

[1] Laboratory of Engineering Mechanics, School of Civil Engineering, Aristotle University of Thessaloniki, GR-54124 Thessaloniki, Greece; ekouris@civil.auth.gr (E.-G.K.); akonsta@civil.auth.gr (A.A.K.); mom@mom.gen.auth.gr (E.C.A.)

[2] School of Civil Engineering, Democritus University of Thrace, GR-67100 Xanthi, Greece; karayan@civil.duth.gr

* Correspondence: lakouris@civil.auth.gr; Tel.: +30-2310-996042

Abstract: The seismic response of five cultural heritage towers erected between the 9th and 10th century AD are investigated herein. Firstly, their architectural and modal characteristics were studied in the light of seismic events that hit the monuments. There exist several historical reports of strong earthquakes, as well as damaged structures and collapses. The limit analysis is adopted to examine the post-elastic behavior of the towers up to collapse due to out-of-plane failure. Recurrent damage modes were collected from recent earthquakes and a classification of four possible collapse mechanisms in towers and slender masonry structures is here proposed: overturning, separation of perpendicular walls, diagonal cracking, and dislocation of the belfry. A thorough examination of the towers under investigation verified the proposed damage classification. The capacity curves were derived combining the capacity curves of each of the collapse mechanisms. Damage thresholds were defined on these curves in correspondence with damage states. The studied group of structures is representative of a wider typology. A statistical approach was adopted to describe damage with seismic intensity, and vulnerability curves were generated. The results of this study will improve the understanding of the performance and the collapse mechanisms of slender masonry structures under seismic loading and provide a characterization of seismic vulnerability for the studied cultural heritage types of towers.

Keywords: cultural heritage towers; campaniles; out-of-plane collapse; limit analysis; displacement spectral capacity; vulnerability

Citation: Kouris, E.-G.; Kouris, L.-A.S.; Konstantinidis, A.A.; Karayannis, C.G.; Aifantis, E.C. Assessment and Fragility of Byzantine Unreinforced Masonry Towers. *Infrastructures* **2021**, *6*, 40. https://doi.org/10.3390/infrastructures6030040

Academic Editor: Maria Pina Limongelli

Received: 18 February 2021
Accepted: 5 March 2021
Published: 9 March 2021

1. Introduction

Unreinforced masonry (URM) structures excited by seismic actions most often form at the ultimate response state an out-of-plane partial collapse mechanism due to weak connections and in-plane cracking [1–4]. It is common knowledge that the main defect of URM walls is their low tensile strength; as a consequence, URM structures tend to create cracks perpendicular to the principal tensile stresses. This inefficiency had been known since ancient times and traditional reinforcement techniques have been developed involving timber and iron ties to mitigate it [3,5–8].

In historic structures, a number of additional critical features, such as high weight/strength ratio, insufficient connection with timber diaphragms, inhomogeneous nature of material, complex constructive stages, lack of rigid diaphragms, presence of vaulted systems, and progressive material degradation due to high compressive stresses, ageing, and environmental influence, dramatically increase their vulnerability. As a result of the inertial forces, the initially monolithic structure is cracked and cut into parts; these parts define the collapse mechanism [9,10]. The interaction among the cracked parts is

often merely simple contact and friction, while in some cases there might be preinstalled joining ties which, depending on their activation level, keep parts connected.

The vibration of a cracked masonry structure, if not adequately tied with any reinforcement (e.g., active tie rods [8] or textiles [11]), contributes in the development of a damage mechanism which brings about collapse. The development of such a collapse mechanism involves the overturning of the most critical part [12]. In these cases the critical part which tends to separate and fail out-of-plane presents a dynamic vibration relevant to that of a rocking rigid body about a constant point [13]. Nevertheless, the vibration of the rocking mechanism is affected by the vibration of the sub-structure which supports it. This has a filtering influence, modifying the characteristics of the ground vibration applied at the foundation [14]. The equation of motion for the rocking response should take into account the interaction with the other elements of the structure, as well as the filtering effect. It has been argued that the assumption of rigid body oscillation is realistic only when masonry is subjected to low-to-moderate compressive vertical loads, otherwise strains are not comparable [15].

Towers made of URM subjected to inertial forces usually collapse by overturning of the most critical part due to insufficient connection between adjacent structural members [16–18]. The uppermost part (i.e., the belfry) is particularly vulnerable to seismic loads when there exist insufficient connections between the piers [19,20]. Other possible collapse mechanisms relate to diagonal cracks or, sometimes, vertical cracks [21]. These cracks have the tendency to separate the integral construction in parts. When a structure is cracked and there is no sufficient connection between the adjacent parts, its dynamic response features a vibration which has the characteristics of a rocking response with simple contact between the parts [13,22–24]. This type of vibration is very frequent in URM towers and leads to out-of-plane collapse.

The vulnerability analysis of historical towers subjected to dynamic actions is a challenging task for two main reasons: (i) masonry's non-linear (NL) behavior is hard to be rigorously modelled due to its complexity; and (ii) accurate material idealization is not straightforward due to the variation of the mechanical properties in a structure. Hence, a number of approaches have been proposed to yield reliable numerical tools capable of as precisely as possible representing the seismic behavior. Finite element (FE) models with plasticity material laws achieve a good accuracy albeit at the expense of a high numerical cost (e.g., [25–32]); thence, their application is limited to only structural members rather than whole structures. Discrete element (DE) models render good results for masonry structures [33–36] but require detailed knowledge of masonry unit arrangement and suffer from accuracy for excessive rotations. Limit analysis has been shown a valuable method to estimate the capacity of masonry structures up to collapse as long as the cracks are effectively described [37–44]. Sophisticated techniques involving dynamic monitoring can reveal the actual state of a traditional masonry structures and points with possible weaknesses [45–55]. Furthermore, building information modelling can be helpful in the investigation of the architectural properties of monumental structures [56].

More than one hundred towers are located on Mount Athos which were erected between the 9th and 10th century AD [57] and are representatives of a large population of similar structures scattered in the area of the erstwhile Byzantine Empire. Some of them were built as defensive structures and observation towers, while others to host bells and in few cases for some other auxiliary purposes [57,58]. Five campaniles of Mount Athos were selected for a thorough study of their seismic vulnerability as they were found to be representative of the respective group. Their heights vary between approximately 20 m to 25 m. Given that our aim is a statistical treatment of the vulnerability and not a specific case-study, a very detailed model is out of the scope of the analysis. Simplified models have been applied to tackle the aforementioned difficulties: (i) simple mechanical models; and (ii) limit analysis [59,60].

In this investigation we adopted these methods based on limit analysis to estimate the displacement capacity and the capacity curves of the towers. In Section 2 the main

properties of the towers are presented. In Section 3 the critical failure mechanisms for cultural heritage towers are reviewed. For those mechanisms, the limit analysis is applied, as well as a displacement procedure, for estimating the respective capacities. The filtering effect of the substructure is investigated in Section 6.1 to convert the capacities into spectral ones. Defining the damage thresholds, we propose a set of fragility curves to describe damage with seismic intensity expressed in terms of spectral displacement in the last section.

2. Characteristics of the Investigated Bell-Towers

2.1. Architectural Features

Five bell-towers were investigated (Figure 1). Table 1 presents the main dimensions: (i) total height; (ii) base height (i.e., the part of the tower with openings); (iii) belfry altitude; (iv) main structure altitude; (v) foundation thickness; (vi) wall thickness (on average); and (vii) footprint area. Hence, the main structure height comes from subtracting the base height from the respective altitude.

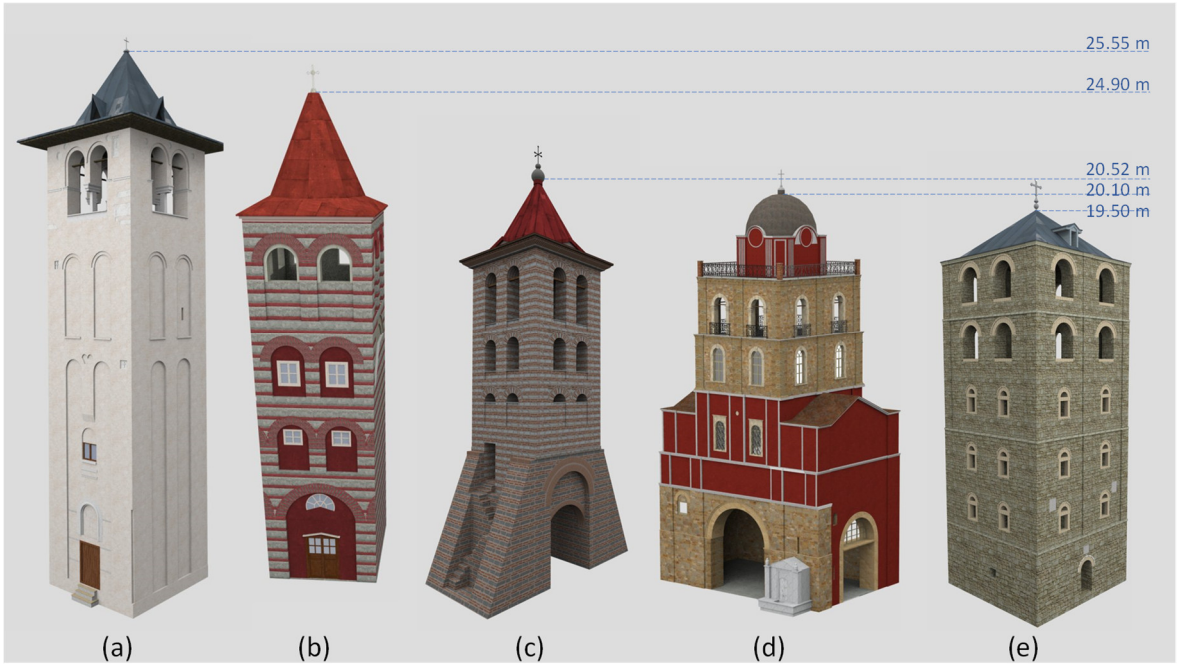

Figure 1. Byzantine bell-towers under investigation: (**a**) Vatopedi, (**b**) Philotheou, (**c**) Protaton, (**d**) Xenophontos, and (**e**) Iveron.

2.1.1. Vatopedi Tower

Among the towers the tallest campanile (25.55 m) is a post-Byzantine tower in the Vatopedi Monastery and dates back to 1427 AD [61]. It is a slender structure with slenderness ratio (i.e., height to width ratio) equal to 5.7 approximately at the uppermost top of the sharp-angled roof (Figure 1a). The height of the masonry structure without the roof structure is 21.0 m. The footprint of the tower is approximately square with a 4.5 m side. The width at the top of the structure is 4.25 m which means that there is a decrease of 25 cm and an inward deflection from the vertical plane of 7‰.

The piers of the structure were constructed from rubble URM carefully bonded. The worked angles are made from quarry faced masonry where the beds and the sides are finely chisel-dressed, but wall faces are roughly worked. Timber beams are embedded at several levels of the structures to improve the connection between perpendicular walls.

The belfry, i.e., the upper part of a bell tower enclosing the bells, is shown in Figure 1a. It has four square piers, sized 90 cm × 90 cm and four intermediate piers half of solid

stone and half of URM. The hip roof is a wooden structure which does not include the timber elements of the initial construction, due to a fire [62].

Table 1. Geometrical characteristics of the case-study bell towers.

	Monasteries	Total Height [m]	Base Height [m]	Belfry Altitude [m]	Main Structure Altitude [m]	Foundation Thickness [m]	Wall Thickness [m]	Area [m²]
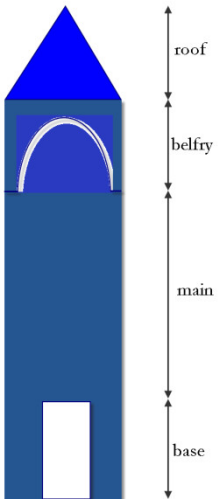	Vatopedi	25.55	7.20	19.00	14.40	1.80	0.85	20.25
	Philotheou	24.90	6.00	18.90	16.50	1.15	1.05	30.25
	Protaton	24.00	7.20	19.00	14.40	1.08	0.85	20.25
	Xenophontos	19.50	2.00	17.00	11.60	1.20	1.05	49.00
	Iveron	20.52	5.00	19.00	17.00	1.05	1.05	45.00

2.1.2. Philotheou Tower

The bell tower of Philotheou Monastery (Figure 1b) is among the oldest built in the 11th century A.D., but it has suffered several interventions and partial reconstructions during the centuries. It is 24.9 m tall and its width measures 5.5 m (see Table 1). Hence, its slenderness ratio is 4.5, lower than that of the Vatopedi tower. The stone masonry is carefully constructed with mortar joints as thick as 7 cm. The walls are 1.15 m thick approximately at the base, slightly decreased at the top (1.05 m). The belfry is 4.5 m high, but the openings are quite small resulting in a robust structure.

2.1.3. Protaton Tower

The Protaton tower (Figure 1c) was first erected in 1534 and later, in 1781, repaired; it follows the architectural characteristics of the most ancient ones. It is a slender structure quite vulnerable due to the presence of a bi-part foundation structure forming an arch. It can be seen as a four-story structure with a total height of 24.0 m. The altitude of the uppermost part of masonry is 20.52 m.

2.1.4. Xenophontos Tower

Xenophontos Monastery was established in 998 AD but the campanile construction started around 1820–1830 and completed on 1 March 1864. The footprint of the structure is square with dimensions 9 × 9 m². The height is 19.50 m. The walls are made of stone masonry. Internal levels are made of timber beams and planks forming five stories (Figure 1d). Tie rods exist at the upper two levels which host the bells. The hip roof is also wooden.

2.1.5. Iveron Tower

The Iveron Monastery (Figure 1e) was established in 980 A.D. but it was destroyed several times due to invasions or, natural catastrophes such as fires and so on. The structure of campanile was restructured around the end of the 19th century and the beginning

of the 20th. Its height is 20.52 m. Its main architectural characteristics are presented in Table 1.

2.2. Modal Properties

Finite element analysis (FEA) was adopted to investigate the modal characteristics of the structures carrying out a modal analysis. ANSYS software was used to model the structure. Hexaedral solid elements (using the element SOLID82) were used for simulation. A refined mesh applying a sensitivity analysis wes carried out with elements around 0.5 m side for URM walls and much finer for the roofs. The meshing for Vatopedi tower is presented in Figure 2 where 2×10^3 elements approximately have been used. The mass of the bells has been added as a point mass attached to the roof. The nodes at the base were assumed fixed as the soil is rocky with high bearing capacity which implies very high stiffnesses for the impedance functions [63].

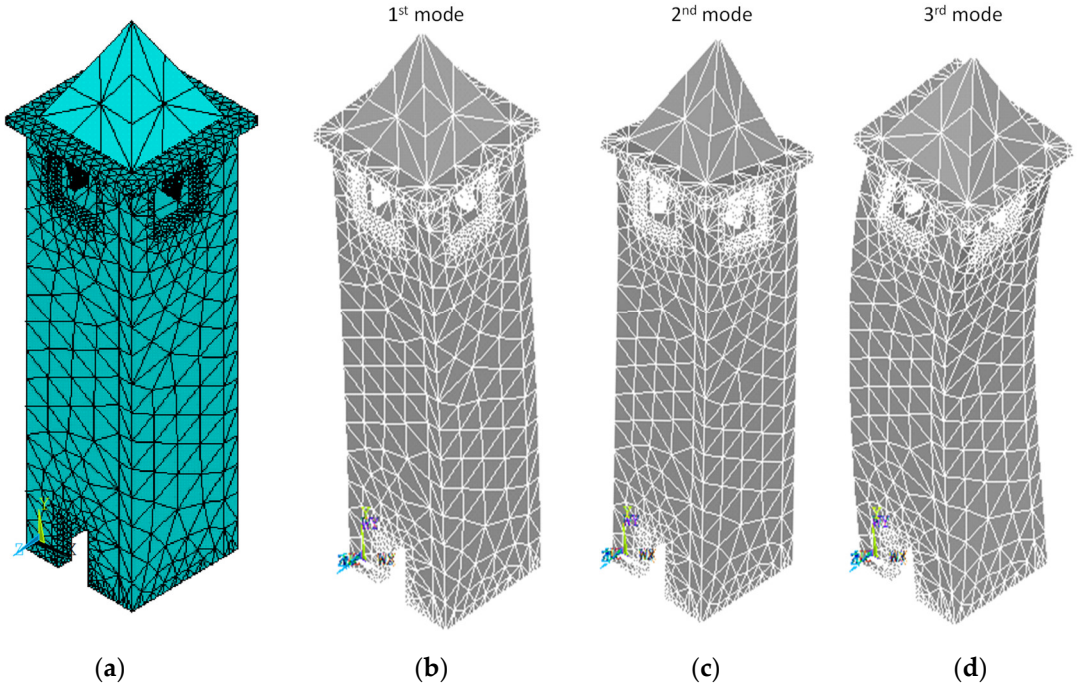

Figure 2. FE simulation of Vatopedi bell-tower: (**a**) meshing, (**b**) 1st modal shape, (**c**) 2nd modal shape, and (**d**) 3rd modal shape.

URM is assumed to be a homogeneous and isotropic material [64–68]. The homogenized elastic modulus [69] and the other properties of masonry were retrieved from the literature [70–74].

The wooden parts of the towers (floors, roof) were assumed to be of class C24 [75] and the respective properties are shown in Table 2. The low value of the elastic modulus reflects the multiphase inhomogeneous and cracked section.

Table 2. Material properties.

	Elastic Modulus [GPa]	**Poisson Ratio**	**Specific Weight [kN/m³]**
Masonry	2.5	0.15	23
Timber	11	0.25	3.5

In the modelling process the following assumptions were made:

- The walls' width is kept constant along the height because variations are considered relatively small;

- The diaphragmatic action of the timber floors and vaults is assumed inactive;
- The mass of the timber floors and vaults is added point-wisely on the URM walls estimating the tributary areas.

The first modal period ranges from 0.29 s for the Xenophontos tower to 0.65 Hz for the Vatopedi tower. The modal periods as well as the modal frequencies for the first three modes are presented in Table 3 [62]. The first two modes have a translational shape in perpendicular axes, while the third one is mostly twisting about the vertical axis.

Table 3. Modal frequencies and periods of towers.

Tower	Modal Periods (s)			Modal Frequencies (Hz)		
	1	2	3	1	2	3
Vatopedi	0.65	0.38	0.08	1.54	2.60	11.89
Xenophontos	0.29	0.14	0.08	3.48	7.26	12.79
Iveron	0.55	0.12	0.09	1.83	8.04	11.26
Protaton	0.34	0.19	0.07	2.92	5.18	14.60
Philotheou	0.44	0.29	0.08	2.28	3.47	12.24

The modal periods estimated from the modal analysis of the FE model in Table 3 are consistent with the values found in the literatures from operational modal analysis [52,66,71,76–90]. Indeed, in these analyses the natural frequency ranges between 0.35Hz for a tower 88 m high in San Gimignano (Italy) [91] up to 4.67Hz for a tower 27.6m in Andrighelli (Italy) [92]. Therefore, the range includes the estimated values of Table 3. Moreover, the tower of Philotheou of 24.90 m height features many similarities with the one of Hagia Sophia in Trapezounta 23 m tall [78], which has a natural frequency 2.08 Hz, i.e., very close to the one found here.

Bartoli et al. [92] proposed the following empirical relationship for the estimation of the natural frequency of towers f_1 from the architectural properties of the towers (L is the side of the tower and H the total heigh) and the velocity of P-waves v_p correlating results from 54 measurements.

$$f_1 \cong \frac{0.15\mathrm{L}}{H^2}\mathrm{v}_p \quad (1)$$

Kouris and Karavezyroglou [17] proposed also an empirical relationship based on the ratio H/L and the modulus of elasticity of the soil E_s:

$$f_1 \cong 0.153\ln(\mathrm{E}_s) + 0.2816(^H/_L) \quad (2)$$

Assuming standard values for rocky soils, v_p = 1000 m/s and E_s = 300 MPa, Equations (1) and (2) yield the modal frequencies for the case-study towers of Table 4. Comparing the values of Tables 3 and 4, a remarkable coincidence is found given the differences of the architectural characteristics of the Protaton tower from the typical tower of the afore-mentioned models.

Table 4. Empirical natural frequencies [Hz] of the towers applying empirical models.

Empirical Equation	Vatopedi	Xenophontos	Iveron	Protaton	Philotheou
1	1.39	3.51	2.27	1.78	2.52
2	1.72	2.04	1.81	2.53	2.45

3. Collapse Mechanisms of Towers

The initially integral structure is cracked due to seismic forces and separates in two or more parts, which constitute the collapse mechanism. These parts interact with one another with simple contact or, develop friction forces.

The elastic or inelastic strains of masonry bodies are very small with respect to the displacements and/or rotations due to free rocking response. Therefore, they can be considered negligible (i.e., rigid body assumption) and not taken into account. This assumption is valid for low-to-moderate vertical loads [15].

It is possible to classify the recurrent types of collapse mechanisms from observations of post-event damage surveys on towers from recent earthquakes [41,62,93]. Damage data from the earthquakes of Friuli (1978) [94] and L'Aquila (2008) [2,95], and Molise (2002) [96] show that there exist four main types of out-of-plane collapse mechanisms: (i) overturning of the tower; (ii) separation of the perpendicular walls; (iii) diagonal cracks and overturning of the critical part; and (iv) dislocation of the belfry. These collapse mechanisms are shown in Table 5.

The first collapse mechanism may appear in slender structures and occurs with a horizontal crack at the base of the structure. The second one appears when the connection between perpendicular walls is very loose. In this case, friction forces develop between key stone units. The third one is very common when diagonal cracks occur. It is reported that this third type can also relate to a vertical crack extending up to the middle diagonally and then, continue vertically splitting in two parts the upper structure [41]; this type is less critical than merely diagonal cracking as it involves friction forces. The last collapse mechanism appears only on bell-towers and is related to the separation of the belfry piers. In the following paragraphs a thorough investigation and a numerical evaluation based on limit analysis of each mechanism is presented.

Table 5. Out-of-plane collapse mechanisms.

Designation	Collapse Mechanism	Out-of-Plane Damage
1 - ANA	Overturning	
2 - APO	Separation of perpendicular wall	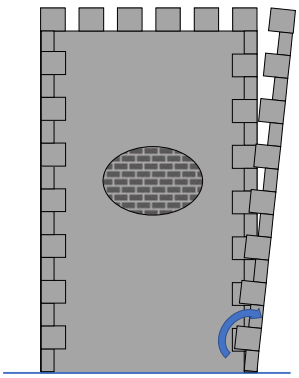

3 - DP	Diagonal cracking	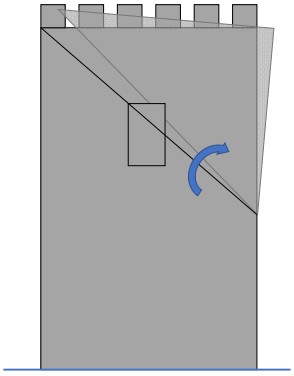
4 - KOP	Dislocation of the belfry	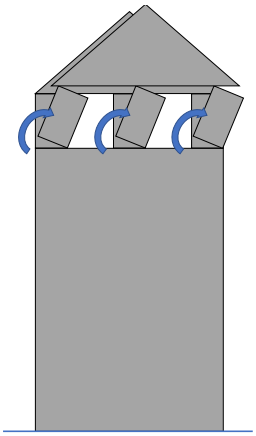

4. Assessment Based on Limit Analysis

4.1. Overturning [1 - ANA]

Towers can be idealized as a simple rectangular structure such as that shown in Figure 3. At the top of the structure there can be an additional mass which represents the bells and the roof mass. A very slender structure can be susceptible to overturning around the base. Our investigation of the first collapse mechanism (ξ = 1 - ANA) is described in the following using the geometric characteristics of Vatopedi tower.

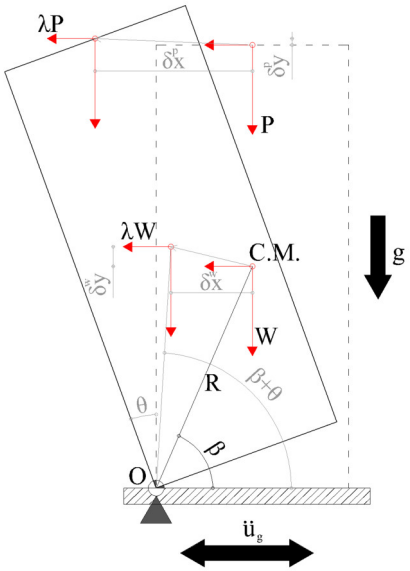

Figure 3. Rocking of a tower at its base.

In the framework of limit analysis, the out-of-plane safety factor λ was estimated simulating the inertia effect with equivalent static forces [41,97,98]. The critical ratio λ of the horizontal actions needed to overturn the tower can be evaluated applying the principle of virtual works for an infinitesimal rotation dθ shown in Figure 3 as follows:

$$\lambda_{\xi=1} = \frac{\sum_i W_{i,x}}{\sum_j W_{j,y}} = \frac{G\dot{\delta}_{y,G} + P\dot{\delta}_{y,P}}{G\dot{\delta}_{x,G} + P\dot{\delta}_{x,P}} \quad (3)$$

In Equation (3), $W_{i,x}$ is the virtual work of the action i in the horizontal direction (x) and $W_{j,y}$ is the virtual work of the action j in the vertical direction (y); G is the gravity force concentrated at the center of gravity of the investigated part and P is the weight of the bells and the roof; $\dot{\delta}_{i,j}$ is the displacement at the i direction $(i = x, y)$ of the j action $(j = G, P)$.

Moment equilibrium would result in an equivalent relation with Equation (3). A wooden staircase twists internally, forming also seven intermediate levels which contributes to Equation (3). G is equal to 2001 kN, P to 5.27 kN and P_1 (i.e., the internal structure) to 3.24 kN. The static forces' horizontal safety factor λ is found equal to 0.34 for this tower (the dimensions are given in Table 1). This value represents the sufficient horizontal force needed to cause the onset of overturning $(\theta = 0°)$ of the gable under static conditions.

The transformation of the rocking rigid body into an equivalent single degree of freedom system (SDOF) system is necessary to compare the capacities of the various mechanisms [99]. The mass of the rocking system is distributed along the height, and is given by the following equation:

$$M^* = \frac{\left(\sum_{i=1}^{N} P_i \Delta_{x,i}\right)^2}{g \sum_{i=1}^{N} P_i \Delta_{x,i}^2} \quad (4)$$

In Equation (4), M^* is the modal mass of the considered first mode and the components of the modal shape are $\Delta_{x,i} = \varphi_{1,i}$. Having assumed that the deformation of the wall is negligible, which is a reasonable assumption for walls tilting around their base, all points are tilting by the same angle θ and the horizontal projection of the displacements $\Delta_{x,i}$ is linear along the height of the wall. The effective modal mass is then found as M^*= 202 ton. The effective mass ratio which is given by the next Equation (5) is equal to 99%.

$$e^* = \frac{gM^*}{\sum_{i=1}^{N} P_i}. \quad (5)$$

The acceleration at the base of the equivalent SDOF system needed to initiate the rocking of the rigid body is given by the maximum value of coefficient λ normalized by the effective mass ratio according to the following expression:

$$a_0^* = \frac{\lambda}{e^*} \quad (6)$$

Equation (6) results in a_0^*= 0.34g. It is well known that a rocking pier possesses a reserve dynamic capacity when subjected to an out-of-plane transient loading [98]. Therefore, the horizontal static multiplier itself is not sufficient to predict the dynamic capacity and hence, it is necessary to further consider the transcendental nature of the seismic excitation.

The principle of virtual work (PVW) for an admissible displacement $\dot{\delta}$ is applied in order to evaluate the minimum value of a static horizontal multiplier of the vertical weights of the building λ that corresponds to the static threshold resistance. The λ_{lim} value is the safety factor of the potential horizontal loading that the structure can support, but for stresses satisfying a strength criterion.

The maximum value of λ represents the necessary inertia at the base of the rocking mechanism to initiate the rotation for the mechanism $(\theta \to 0°)$ which is found solving

Equation (3) for $\theta \to 0°$. As the rotation θ increases, λ will drop to zero. This instant represents the ultimate condition for rocking of the mechanism and sets off the collapse state due to overturning.

The maximum rotation θ of the vibrating gable mechanism before collapse was calculated from Equation (3) for λ = 0. This value was found to be equal to θ_{ult} = 0.20 rad for the first collapse mechanism (ξ = 1 - ANA) through an iterative procedure consisting of a stepwise gradual increase of $\dot{\delta}$ and estimating the resulting λ. Using the properties of the first mode, the displacement capacity d^* for the equivalent SDOF results from the top displacement of the mechanism multiplied by the inverted modal participation factor of the first mode Γ_1^{-1} applying the following expression similar to Equation (4) for mass:

$$d_0^* = d_k \frac{\sum_{i=1}^{n+m} P_i \Delta_{x,i}^2}{\Delta_{x,k} \sum_{i=1}^{n+m} P_i \Delta_{x,i}} = d_k \frac{\Gamma_1^{-1}}{\Delta_{x,k}}. \quad (7)$$

In Equation (7) above, d_k is the relative displacement at the control point of the collapse mechanism and $\Delta_{x,i}$ are the modal coordinates of the various weights P_i. The modal coordinates are considered equivalent to modal displacements and were normalized against the top modal displacement value (i.e., $\Delta_{x,k}$). The SDOF coefficient of Equation (7), i.e., the normalized modal participation factor $\Gamma_1^{-1}/\Delta_{x,k}$, is equal to 0.50 for the overturning of the tower. The maximum displacement of the equivalent SDOF system d_0^* would be 1.25 m. However, the ultimate displacement of the gable walls collapse mechanism should be further reduced to consider inherent physical conditions that would force the mechanism to collapse before the maximum displacement is attained; an example is the unseating of beams supporting floors which may cause collapse before the ultimate displacement is reached. Comparisons with NL analyses and experimental results have shown that the maximum displacement of the equivalent SDOF system d_0^* should be reduced by 40-50% [38,100]. This reduction would result in an ultimate displacement of the collapse mechanism (40%) · $d_0^* = d_u^*$ = 0.50 m. The resulting capacity curve for collapse mechanism is presented in Figure 4. It can be seen that the capacity curve is bilinear with the second branch having a constant negative slope.

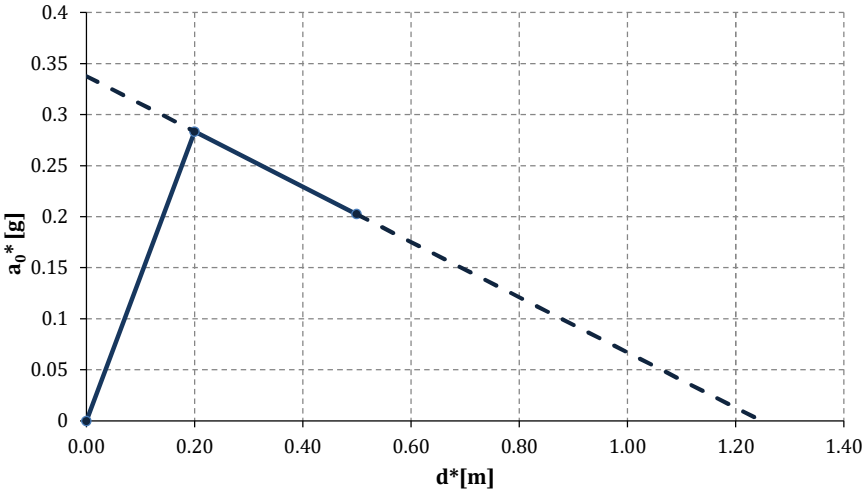

Figure 4. Capacity curve for collapse mechanism 1 - ANA of the Vatopedi tower.

The equivalent SDOF systems with the capacity curve shown in Figure 4 is not characterized by a unique natural frequency as their non-linear response suggests. However, these non-linear systems can be idealized with an equivalent linear SDOF system having an effective natural period which maximizes the response. This appears in a fraction of the ultimate displacement, which according to [40,99] is at the 40% of the ultimate displacement (0.20 m) and, the effective acceleration corresponding to the effective displacement a_s^* is identified on the capacity curve (a_s^* = 0.28 g = 2.79 m/s²) the effective secant

period $T_s = 2\pi(M/K)^{1/2}$ was calculated using the secant properties of the equivalent SDOF elastic system [101,102]. The effective secant period was found to be 1.68 s.

Obviously, the less slender the tower the less critical the overturning collapse mechanism. Moreover, other local instabilities, e.g., the delamination of multi-leaf masonry walls due to heterogeneity, may trigger other failure modes. The geometry of the bell-tower of Iveron Monastery make it unsusceptible to overturning.

4.2. Separation [2 - APO]

This second type of collapse mechanism (Table *5*) is always accompanied by sliding of stone units and development of friction forces F_{fr}. The Mohr-Coulomb friction law is adopted (F_{fr} = μ·σ) assuming conservatively that the cohesion modulus *c* is zero as this is the case for long standing monuments experiencing several earthquakes during their history, and the friction coefficient μ is equal to 0.4 according to Eurocode-6 [103]. Equation (3) is modified to include the frictional forces as follows:

$$\lambda_{\xi=2} = \frac{\sum_n F_{fr,n}\dot{\delta}_{x,n} + \sum_i P_i\dot{\delta}_{y,i}}{\sum_i P_i\dot{\delta}_{x,i}} \quad (8)$$

In Equation (8) above *n* is the number of stone units at the corner along the height of the tower. These units are assumed to have equal dimensions although it is known that in general this is not the case for stone units. The average height of the stone units is assumed equal to 0.35 m. Equation (8) is solved in an iterative and stepwise manner according to the following steps:

- $\dot{\delta}$ is increased by a specified step;
- Vertical stresses σ in the contact areas are estimated;
- Friction forces F_{fr} are estimated;
- The static forces safety factor λ is estimated;
- If λ is negative the specified step is decreased to reach a balance ($\lambda = 0$).

The above iterative solution of Equation (8) is non-linear, resulting in the capacity curve shown in Figure 5, where d_0^* is found to be 0.43 m, d_u^* equal to 0.17 m and d_s^* equal to 0.07 m.

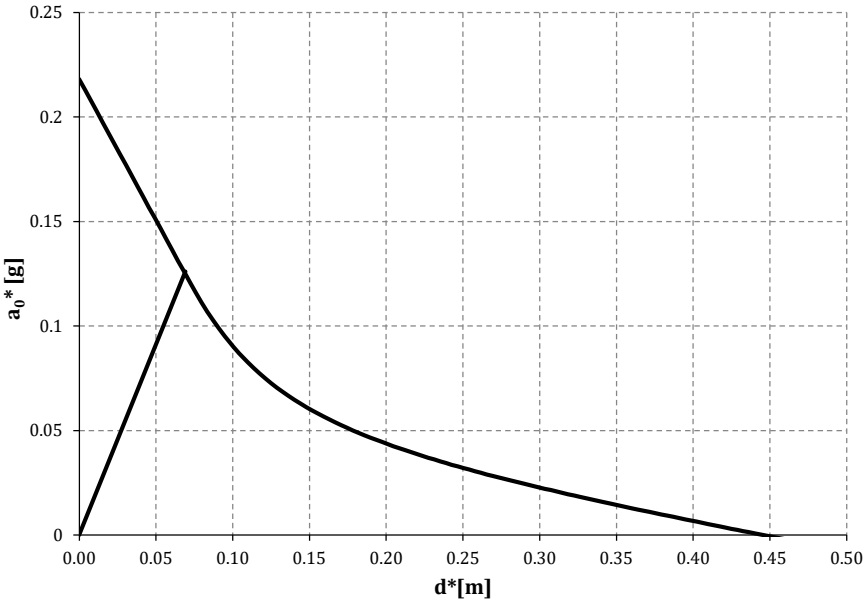

Figure 5. Capacity curve for collapse mechanism 2 - APO of the Vatopedi tower.

4.3. Diagonal Cracking [3 - DR]

Diagonal in-plane cracks can be the triggering cause of out-of-plane collapse of stone URM structures [104]. The inclination of the cracks depends on: (i) the stress field; (ii) the bonding of the stone units; and (iii) openings in the walls. It is assumed that the inclination of the cracks is 45^0. Moreover, the diagonal crack may appear anywhere along the height of the structure. For example, in Figure 6 two extreme positions are shown: (i) at the left the crack is at the top of the structure ($\Delta z = 0.1H$); and (ii) at the right the crack is at the bottom ($\Delta z = H$).

Figure 6. Two possible diagonal cracks (in black) along the height of the Vatopedi tower.

To identify the critical position Δz of the diagonal crack, a parametric analysis was carried out examining cracks in several elevations ($0 < \Delta z \leq H$) as presented in Figure 7. The maximum acceleration a_{max} needed to cause the out-of-plane collapse was found to be the one at the highest elevation. On the contrary, when the diagonal crack occurs at the base, only 20% of a_{max} would be sufficient to cause collapse (Figure 7). Therefore, diagonal cracks at the base are more critical—something which has been observed in several earthquakes [105]. However, local deficiencies and openings may alter the position of the critical cracks [16]. The procedure to estimate the critical acceleration ($a_{max} = \lambda \cdot g$) is based on Equation (3) accordingly modified for triangular (or more complicated) structural parts [13,62].

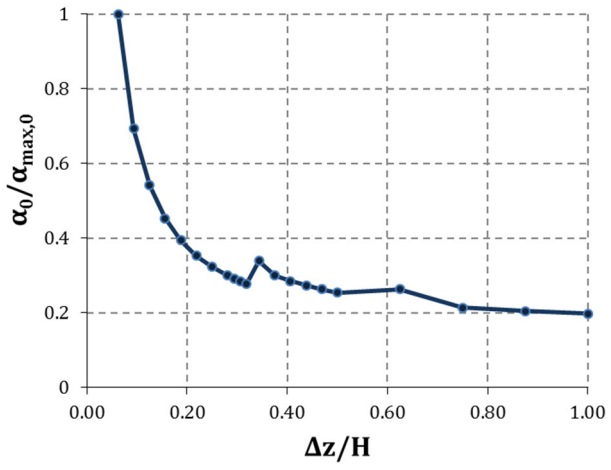

Figure 7. Variation of the acceleration needed to cause out-of-plane collapse.

4.4. Dislocation of the Belfry [4 - KOR]

The last collapse mechanism in bell towers is related to the failure of the piers of the belfry [85]. The large openings of the upper part of the tower make them very vulnerable structures. Simplified models to investigate the vulnerability of belfries have been proposed in [106]. The collapse may occur due either: (a) rocking of one pier and sliding of the other; or (b) rocking of both of them as shown in Figure 8.

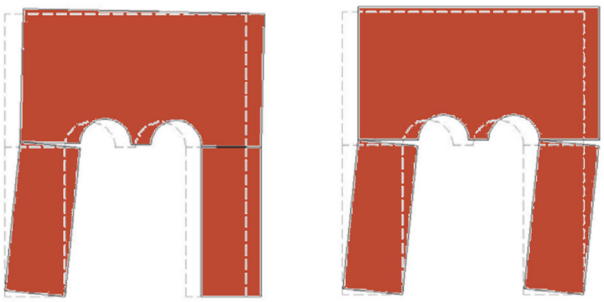

(**a**) (**b**)

Figure 8. Variation of the acceleration needed to cause out-of-plane collapse.

For the first type of belfry collapse mechanism (Figure 8a) friction forces participate in the equilibrium and thus, Equation (8) was applied. For the second type (Figure 8b) and due to the symmetry of the forces, the problem is confined to the rocking of one pier and Equation (3) was used. The respective capacity curves are presented in Figure 9a,b where it is clearly seen that the second type is more critical.

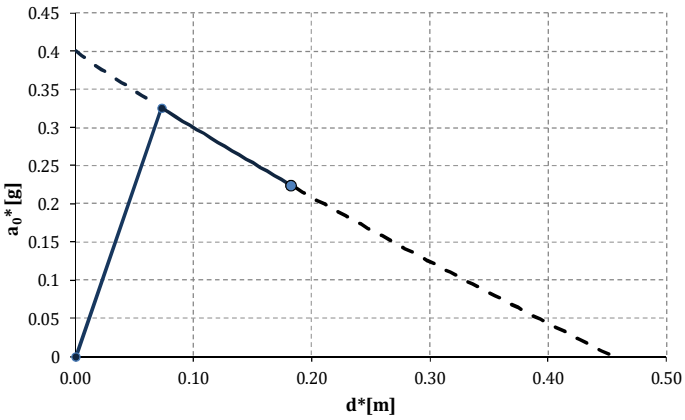

(**a**)

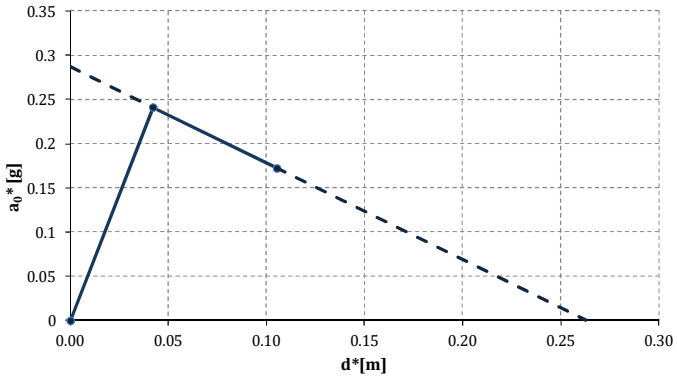

(**b**)

Figure 9. Capacity curves of Protaton belfry: (**a**) rocking and sliding, and (**b**) only rocking.

5. Filtering Effect

When the collapse mechanism involves a part of the structure standing at a certain elevation, as in the case of belfries, the spectral acceleration capacity should be estimated taking into account the filtering effect of the substructure. The underlying structure acts as a filter of the base motion modifying the frequency characteristics of the base excitation given by the transfer function $H(T_s, T_1)$. A number of expressions have been proposed to estimate the floor response spectrum (FRS) given the base response spectrum and the dynamic characteristics of the structure (e.g., [14,107,108]).

A simplified expression of the transfer function $H(T_s, T_1)$to estimate the filtering effect of the underlying structure is given by the next expression [38]:

$$H = \begin{cases} T_s < T_1: |\psi_1(Z)|\gamma_1 \dfrac{(T_s/T_1)^2}{\left[(1-T_s/T_1)^2 + \left[0.05(T_s/T_1)/\left(\eta(\xi_s)\eta(\xi_1)\right)\right]\right]^{1/2}} \\ T_1 < T_s < 1.9T_1: \eta(\xi_s)\eta(\xi_1)|\psi_1(Z)|\gamma_1 \dfrac{(T_s/T_1)^2}{\left[(1-T_s/T_1)^2 + [0.05(T_s/T_1)]\right]^{1/2}} \\ T_s > 1.9T_1: 3.8\eta(\xi_s)\eta(\xi_1)|\psi_1(Z)|\gamma_1 \end{cases} \quad (9)$$

In Equation (9), $\psi_1(Z)$ is the shape of the fundamental mode of vibration of the building in the direction considered, normalised to the displacement at the top of the building. A reasonable approximation of the fundamental mode of masonry regular buildings is given by the ratio (Z/H) in which H stands for the height of the structure measured and Z stands for the elevation of the center of gravity of the mechanism. In Equation (9), γ_1 is the corresponding modal participation factor which depends of the number of internal floors n [109]: $\gamma_1 = 3n/(2n+1)$. Using this expression, the spectral capacities have been estimated and are presented on the last column of Table 6.

6. Seismic Response

6.1. Capacity Curves

The final capacity curve of each tower is a segmented curve joining the critical parts of each mechanism. For instance, the capacity curve of Philotheou tower is a bipartite curve involving the diagonal cracking of the walls and the dislocation of the belfry (type-a) as presented in Figure 10.

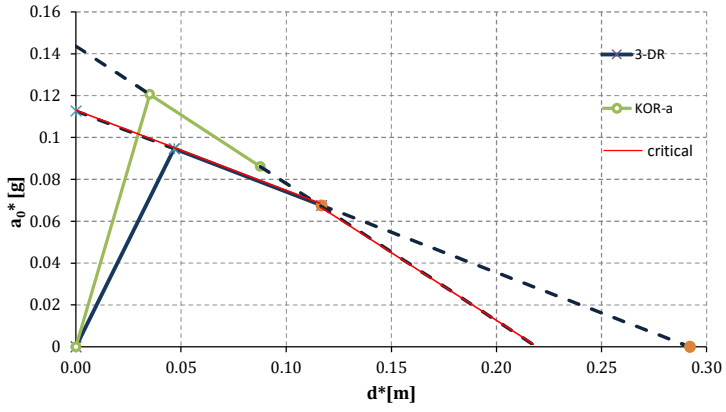

Figure 10. Capacity curve for Philotheou tower.

Following the methodology described in the previous sections, the spectral capacity curves for all the mechanisms were derived indicating the final critical capacity curve and are presented in Figure 11 for the group of towers. The critical collapse mechanism of the Vatopedi bell tower is mainly formed due to dislocation of the belfry [4 - KOR] followed

by the diagonal cracking (Figure 11a). The capacity curves of Philotheou tower for all the mechanisms are shown in Figure 11b.

The arch of the Protaton bell tower is assumed to avoid damage not participating in the failure, and hence the collapse mechanisms occur higher than 4.45 m (the elevation of the arch). Then, using Equation (7) the final capacities curves were derived (Figure 11c). The critical curve is composed by a sequence starting from the second, and then moving to the fourth and at the final part to the third collapse mechanisms.

A similar sequence of collapse applies also to Xenophontos bell tower in which the [2 - APO] is also very near to the critical (Figure 11d). For Caracallou tower the [3 - DR] is the critical mechanism followed at a certain point by the [2 - APO] (Figure 11e). Finally, the Iveron bell towers present a critical collapse mechanism which coincides with the diagonal failure [3 - DR].

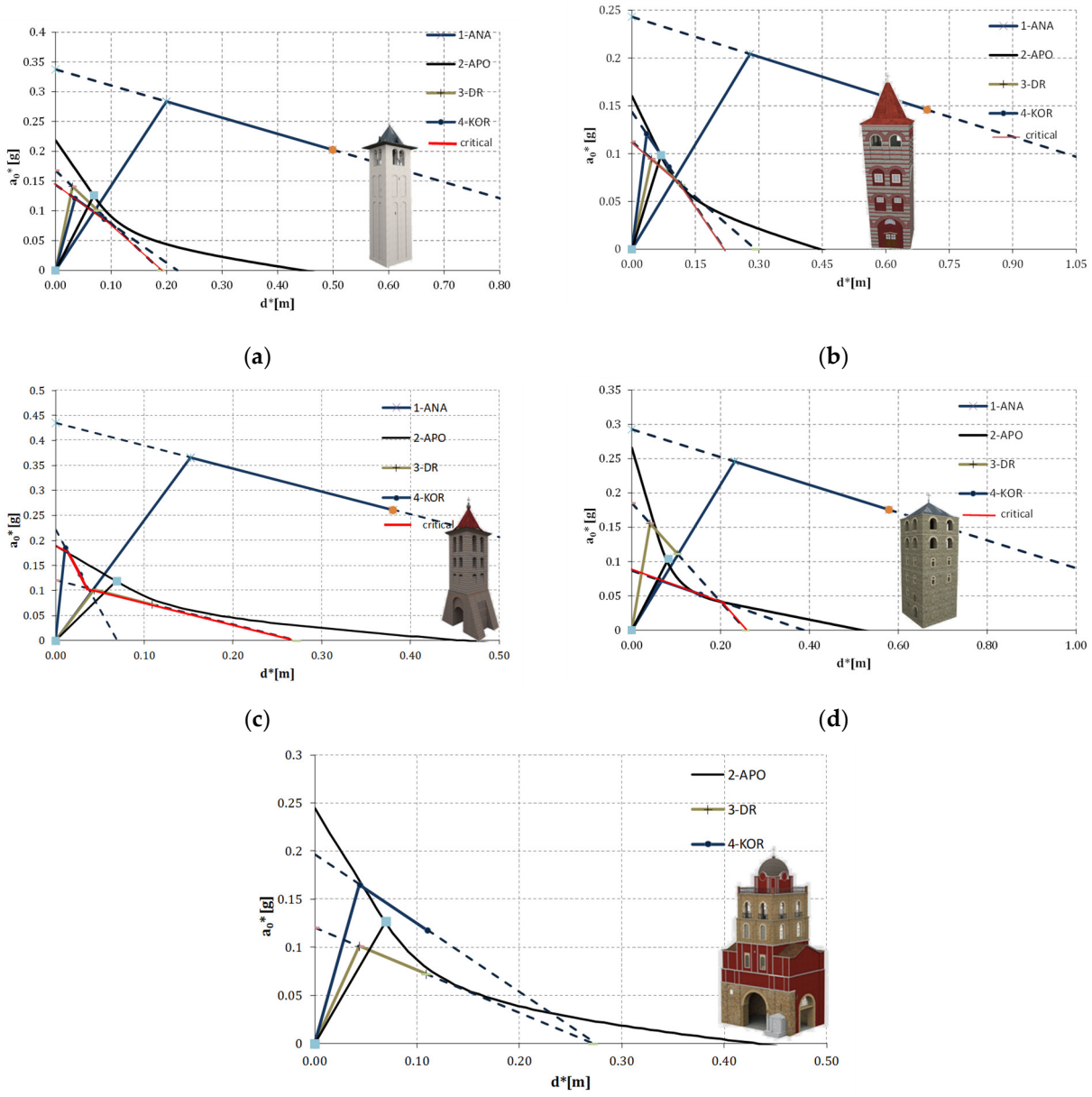

Figure 11. Capacity curves: (**a**) Vatopedi tower, (**b**) Philotheou bell tower, (**c**) Protaton tower, (**d**) Xenophontos bell tower, and (**e**) Iveron bell tower.

The ultimate displacements of each mechanism and the effective secant period of the most critical one for each tower are presented in Table 6. In the last column of the table the spectral value of the most critical mechanism is presented.

Table 6. Out-of-plane collapse mechanisms: spectral displacements.

Tower	Eff. Period (s)	Displacement Capacity (cm)				
		1 - ANA	2 - APO	3 - DR	4 - KOR	Spectral Displacement [1]
Vatopedi	0.84	50	17	11	29	8
Philotheou	2.41	73	17	11	41	11
Protaton	2.25	38	17	11	41	13
Xenophontos	1.49	58	21	20	20	10
Iveron	2.20	-	18	14	41	12

[1] Taking into account the filtering effect (Equation (9)).

The estimated displacement capacities of the towers were compared to the displacement demands that the earthquakes impose. The gradual cracking in recurrent seismic events leads to higher effective periods than those natural elastic in Table 3. Seismic codes usually focus only on acceleration spectra. The estimation of the displacement spectrum is usually based on pseudo-spectral conversion $S_D = S_A(T/2\pi)^2$, where S_D and S_A are the spectral displacement and acceleration respectively. However, this estimation is approximate and leads to errors for high periods [110,111]. The following expressions were used for the estimation of the corner period T_c and the maximum spectral displacement δ_{max} in relation to the earthquake magnitude M_w and the epicentral distance r [111].

$$T_C = 1 + 2.5(M_w - 5.7) \quad (10a)$$

$$\delta_{max} = C_s \frac{10^{(M_w - 3.2)}}{r} \quad (10b)$$

In Equations (10), T_c is given in s and δ_{max} is in mm and C_s is a coefficient which for a firm soil becomes unity. Two extreme scenarios can be examined from the seismicity of the region [112,113] to establish the spectral demand: (a) a magnitude 6.2 from an epicentral distance 15 km; and (b) a magnitude 7.2 from an epicentral distance 100 km. The displacement demands for the estimated period are the green shadowed area ranging between approximately 3 and 7 cm in Figure 12. The estimated capacities show the displacement reserve that the towers possess in avoiding failure.

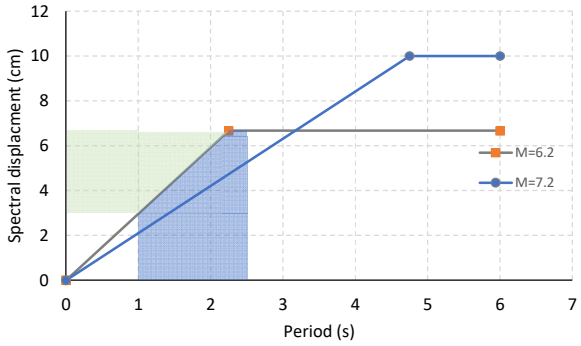

Figure 12. Displacement spectral demand for two earthquakes with magnitudes 6.2 and 7.2.

6.2. Vulnerability Curves

Fragility curves describing the evolution of damage can be based on a (cumulative) lognormal distribution [114–118]. The cumulative lognormal fragility curves are dependent on two parameters: the mean value m_i of the spectral displacement and its standard deviation σ_i of each limit state i. Statistical simulations such as Monte-Carlo analyses can be used to determine the mean value and the standard deviation [41]. Here however, a simper procedure was followed using the capacity curves previously derived: Lagomarsino [99] suggested four damage states defined on the capacity curves. The second damage state coincides with the elastic limit ($m_2 = d_s^*$) while the fourth one with the ultimate displacement ($m_4 = d_s^*$). The other two damage states are defined in respect to the first ($m_1 = 0.7$, $m_2 = 0.7\ d_s^*$) and to the fourth ($m_3 = 0.4$, $m_4 = 0.4\ d_u^*$). To derive the capacity curve the mean and the standard deviation of each damage states were estimated.

The standard deviation can be assumed that corresponds to the uncertainty due to the definition of the damage states $\beta_{T,ds,i}$ (see Table 6). Two other sources of uncertainty should be also considered: (i) the variability due to the ground motion β_D; and (ii) the variability due to the response of the structure β_C.Assuming a statistical independency of the various sources of variability, the total variability should be the square root of the sum of their squares. It was assumed here that the convolved variability $\beta_{CONV(C,D)}$of these contributors is 0.7, based on the proposed values of HAZUS [119]. Therefore, the variability of each damage state $\beta_{ds,i}$ should be equal to $\left(0.7^2 + \beta_{T,ds}^2\right)^{1/2}$. Using this relation, a variability value is estimated which is used together with the mean values to generate a general set of vulnerability curves for towers regardless the specific characteristics of the various categories (Figure 13). The lognormal distribution was applied. The statistical values of the damage states are presented in Table 7.

Table 7. Mean (m_i) and standard deviations $\beta_{T,ds,i}$ of damage state i (m).

i	Mean	$\beta_{T,ds,i}$	$\beta_{ds,i}$
1	0.01	0.01	0.70
2	0.02	0.02	0.70
3	0.06	0.03	0.70
4	0.11	0.05	0.70

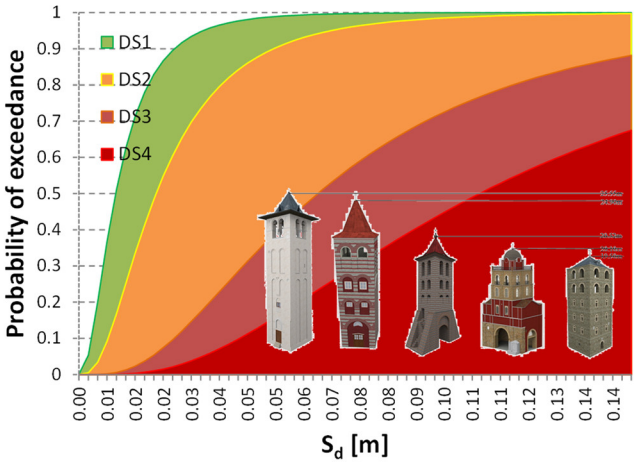

Figure 13. Vulnerability curves for the towers.

7. Conclusions

A group of Byzantine towers was examined with the purpose to assess their out-of-plane failure capacity and provide seismic fragility curves for quick estimates. The towers are located on Mount Athos, Greece and represent a large population of cultural heritage

defense and monastic slender structures. Historical evidence reveals the possible collapse mechanisms of the towers. The four critical failure mechanisms historically witnessed are: (i) the overturning; (ii) the separation of the perpendicular walls; (iii) the diagonal cracking; and (iv) the dislocation of the belfry in the case of bell towers. The capacity curves of the towers were estimated applying the limit analysis together with a displacement-based methodology of the collapse mechanisms. For each collapse mechanism a capacity curve was associated. The capacity curve of the tower is a segmented curve comprised of the critical parts of the respective curves. Damage states were defined in relation to the capacity curves. Following this procedure, capacity curves have been derived for the group of towers under investigation and the mean values and the standard deviations have been estimated for the damage states. Using these values, a set of vulnerability curves expressed in terms of spectral displacement have been proposed, which are proposed for cultural heritage structures with similar characteristics.

Author Contributions: Conceptualization, methodology, L.-A.S.K. and E.-G.K.; software, validation, formal analysis, investigation, data curation, writing—original draft preparation, E.-G.K.; original draft editing, L.-A.S.K., A.A.K., C.G.K. and E.C.A.; revision and re-organization of original draft, E.C.A., C.G.K. and L.-A.S.K.; supervision, E.C.A.; funding acquisition, E.-G.K. All authors have read and agreed to the published version of the manuscript.

Funding: This research was funded by IKY Fellowships of Excellence for Postgraduate Studies in Greece -Siemens Program, grant number SPHD/11167/13b.

Data Availability Statement: The data presented in this study are available on request from the corresponding author.

Acknowledgments: E.C.A. has been supervising the PhD research of E.-G.K. and C.G.K. and A.A.K. were in the advisory committee. L.-A.S.K. has contributed with his expertise in the field, throughout this research.

Conflicts of Interest: The authors declare no conflict of interest.

References

1. Ferreira: T.M.; Costa, A.A.; Costa, A. Analysis of the Out-Of-Plane Seismic Behavior of Unreinforced Masonry: A Literature Review. *Int. J. Arch. Herit.* **2014**, *9*, 949–972.
2. Indirli, M.; Kouris, L.A.S.; Formisano, A.; Borg, R.P.; Mazzolani, F.M. Seismic Damage Assessment of Unreinforced Masonry Structures After the Abruzzo 2009 Earthquake: The Case Study of the Historical Centers of L'Aquila and Castelvecchio Subequo. *Int. J. Arch. Herit.* **2013**, *7*, 536–578, doi:10.1080/15583058.2011.654050.
3. Kouris, L.A.S.; Borg, R.P.; Indirli, M. The L'Aquila Earthquake, April 6th, 2009: A Review of Seismic Damage Mechanisms. In Proceedings of the COST ACTION C26: Urban Habitat Constructions Under Catastrophic Events—Proceedings of the Final Conference, Naples, Italy, 16–18 September 2010; Mazzolani, F.M., Ed.; Taylor & Francis Group: London, UK, 2010; pp. 673–681.
4. Borg, R.P.R.; Indirli, M.; Rossetto, T.; Kouris, L.A. L'Aquila Earthquake April 6th, 2009: Damage Assessment Methodologies. In Proceedings of the Urban Habitat Constructions under Catastrophic Events, Naples, Italy, 16–18 September 2010; Mazzolani, F.M., Ed.; Taylor & Francis Group: London, UK, 2010; pp. 557–564.
5. Kouris, L.A.S.; Kappos, A.J. Detailed and simplified non-linear models for timber-framed masonry structures. *J. Cult. Herit.* **2012**, *13*, 47–58, doi:10.1016/j.culher.2011.05.009.
6. Kouris, L.A.; Kappos, A.J. Seismic Performance of Ancient Timber-Framed Walls. In Proceedings of the 4th International Congress: Science and Technology for the Safeguard of Cultural Heritage of the Mediterranean Basin, Cairo, Egypt, 6–8 December 2009; Ferrari, A., Ed.; CNR, Inst. of Chemical Methodologies: Rome, Italy, 2009; Volume 3, pp. 119–127.
7. Kouris, L.A.S.; Kappos, A.J. Numerical Investigation and Empirical Seismic Vulnerability Assessment of Timber- Framed Masonry Buildings. ISBN 9781466682870/1466682868/9781466682863. 2015. Available online: https://www.scienceopen.com/book?vid=03549d92-5059-4d17-a6a1-70290a881f96 (accessed on 14 March 2017).
8. Kouris, E.; Kouris, L. Investigation of the Influence of Tie-Rods on the Seismic Behaviour of Slender Towers. *Proc. Twelfth Int. Conf. Comput. Struct. Technol.* **2014**, *106*, doi:10.4203/ccp.106.80.
9. Augusti, G.; Ciampoli, M.; Giovenale, P. Seismic vulnerability of monumental buildings. *Struct. Saf.* **2001**, *23*, 253–274, doi:10.1016/s0167-4730(01)00018-2.
10. Giordano, A.; De Luca, A.; Mele, E.; Romano, A. A simple formula for predicting the horizontal capacity of masonry portal frames. *Eng. Struct.* **2007**, *29*, 2109–2123, doi:10.1016/j.engstruct.2006.10.011.

11. Kouris, L.A.S.; Triantafillou, T.C. State-of-the-art on strengthening of masonry structures with textile reinforced mortar (TRM). *Constr. Build. Mater.* **2018**, *188*, 1221–1233, doi:10.1016/j.conbuildmat.2018.08.039.
12. Mele, E.; De Luca, A.; Giordano, A. Modelling and analysis of a basilica under earthquake loading. *J. Cult. Herit.* **2003**, *4*, 355–367, doi:10.1016/j.culher.2003.03.002.
13. Giresini, L.; Fragiacomo, M.; Sassu, M. Rocking analysis of masonry walls interacting with roofs. *Eng. Struct.* **2016**, *116*, 107–120, doi:10.1016/j.engstruct.2016.02.041.
14. Menon, A.; Magenes, G. Definition of Seismic Input for Out-of-Plane Response of Masonry Walls: I. Parametric Study. *J. Earthq. Eng.* **2011**, *15*, 195–213.
15. Lam, N.; Griffith, M.; Wilson, J.; Doherty, K. Time–history analysis of URM walls in out-of-plane flexure. *Eng. Struct.* **2003**, *25*, 743–754, doi:10.1016/s0141-0296(02)00218-3.
16. Preciado, A.; Sperbeck, S.T.; Ramírez-Gaytán, A. Seismic vulnerability enhancement of medieval and masonry bell towers externally prestressed with unbonded smart tendons. *Eng. Struct.* **2016**, *122*, 50–61, doi:10.1016/j.engstruct.2016.05.007.
17. Kouris, S.S.; Weber, M.K.K. Numerical Analysis of Masonry Bell-Towers under Dynamic Loading. *J. Civ. Eng. Arch.* **2011**, *5*, 715–722.
18. Kouris, S.S.; Karaveziroglou-Weber, M. Research on the Seismic Strengthening of a Medieval Masonry Campanile. *Struct. Eng.* **2009**, *87*, 20–24.
19. Casolo, S.; Milani, G.; Uva, G.; Alessandri, C. Comparative seismic vulnerability analysis on ten masonry towers in the coastal Po Valley in Italy. *Eng. Struct.* **2013**, *49*, 465–490, doi:10.1016/j.engstruct.2012.11.033.
20. Ubertini, F.; Cavalagli, N.; Kita, A.; Comanducci, G. Assessment of a monumental masonry bell-tower after 2016 Central Italy seismic sequence by long-term SHM. *Bull. Earthq. Eng.* **2018**, *16*, 775–801, doi:10.1007/s10518-017-0222-7.
21. Kouris, S.S.; Karaveziroglou-Weber, M.K. Structural Analysis and Diagnosis of Masonry Towers. In *Proceedings of the ECCOMAS Thematic Conference—COMPDYN 2011: 3rd International Conference on Computational Methods in Structural Dynamics and Earthquake Engineering: An IACM Special Interest Conference*; Papadrakakis, M., Fragiadakis, M., Plevris, V., Eds.; National Technical University of Athens: Athens, Greece; 2011.
22. Landi, L.; Gabellieri, R.; Diotallevi, P.P. A model for the out-of-plane dynamic analysis of unreinforced masonry walls in buildings with flexible diaphragms. *Soil Dyn. Earthq. Eng.* **2015**, *79*, 211–222, doi:10.1016/j.soildyn.2015.09.013.
23. Abrams, D.P. RESPONSE OF UNREINFORCED MASONRY BUILDINGS. *J. Earthq. Eng.* **1997**, *1*, 257–273, doi:10.1080/13632469708962368.
24. Portioli, F.; Casapulla, C.; Cascini, L.; D'Aniello, M.; Landolfo, R. Limit analysis by linear programming of 3D masonry structures with associative friction laws and torsion interaction effects. *Arch. Appl. Mech.* **2013**, *83*, 1415–1438, doi:10.1007/s00419-013-0755-4.
25. Pasiou, E.D.; Kourkoulis, S.K. Mechanical response of marble epistyles under shear: Numerical analysis using an experimentally validated model. *J. Mech. Behav. Mater.* **2018**, *27*, 27, doi:10.1515/jmbm-2018-0023.
26. Kouris, L.A.; Valsamos, G.; Triantafyllou, S.; Karlos, V.; Pohoryles, D.A.; Bournas, D.A.; Larcher, M.; Casadei, F. Protection of Masonry Structures against Explosions Applying Layers of Textile Reinforced Mortar. In Proceedings of the International Conference on Structural Dynamic, EURODYN, Athens, Greece, 13–25 November 2020; Papadrakakis, M., Fragiadakis, M., Papadimitriou, C., Eds.; National Technical University of Athens (NTUA): Athens, Greece, 2020; Volume 2, pp. 2573–2584.
27. Kouris, L.A.S. Practical Simulation Tools for the Seismic Analysis of Timber-Framed Masonry Structures. In *Historical Earthquake-Resistant Timber Frames in the Mediterranean Area*; Ruggieri, N., Tampone, G., Zinno, R., Eds.; Springer: Cham, Switzerland; 2013.
28. Kouris, L.A.S.; Meireles, H.; Bento, R.; Kappos, A.J. Simple and complex modelling of timber-framed masonry walls in Pombalino buildings. *Bull. Earthq. Eng.* **2014**, *12*, 1777–1803, doi:10.1007/s10518-014-9586-0.
29. Kouris, L.A.S.; Kappos, A.J. A practice-oriented model for pushover analysis of a class of timber-framed masonry buildings. *Eng. Struct.* **2014**, *75*, 489–506, doi:10.1016/j.engstruct.2014.06.012.
30. Habieb, A.B.; Valente, M.; Milani, G. Effectiveness of different base isolation systems for seismic protection: Numerical insights into an existing masonry bell tower. *Soil Dyn. Earthq. Eng.* **2019**, *125*, 105752, doi:10.1016/j.soildyn.2019.105752.
31. Shehu, R. Preliminary Assessment of the Seismic Vulnerability of Three Inclined Bell-towers in Ferrara, Italy. *Int. J. Arch. Herit.* **2020**, 1–33, doi:10.1080/15583058.2020.1805045.
32. Pintucchi, B.L.; Zani, N. Effectiveness of nonlinear static procedures for slender masonry towers. *Bull. Earthq. Eng.* **2014**, *12*, 2531–2556, doi:10.1007/s10518-014-9595-z.
33. Gambarotta, L.; Lagomarsino, S. Damage Models for the Seismic Response of Brick Masonry Shear Walls. Part II: The Continuum Model and Its Applications. *Earthq. Eng. Struct. Dyn.* **1997**, *26*, 423–439.
34. Psycharis, I.N.; Lemos, J.V.; Papastamatiou, D.Y.; Zambas, C.; Papantonopoulos, C. Numerical study of the seismic behaviour of a part of the Parthenon Pronaos. *Earthq. Eng. Struct. Dyn.* **2003**, *32*, 2063–2084, doi:10.1002/eqe.315.
35. Lemos, J.V. Discrete Element Modeling of Masonry Structures. *Int. J. Arch. Herit.* **2007**, *1*, 190–213, doi:10.1080/15583050601176868.
36. Ferrante, A.; Clementi, F.; Milani, G. Dynamic Behavior of an Inclined Existing Masonry Tower in Italy. *Front. Built Env.* . **2019**, *5*, 33, doi:10.3389/fbuil.2019.00033.
37. Peña, F.; Prieto, F.; Lourenço, P.B.; Campos Costa, A.; Lemos, J.V. On the Dynamics of Rocking Motion of Single Rigid-Block Structures. *Earthq. Eng. Struct. Dyn.* **2007**, *36*, 2383–2399.

38. Lagomarsino, S. Seismic assessment of rocking masonry structures. *Bull. Earthq. Eng.* **2015**, *13*, 97–128, doi:10.1007/s10518-014-9609-x.
39. Sorrentino, L.; Masiani, R.; Benedetti, S. Experimental Estimation of Energy Damping during Free Rocking of Unreinforced Masonry Walls. First Results. *Aip Conf. Proc.* **2008**, *1020*, 1888–1895, doi:10.1063/1.2963825.
40. Doherty, K.; Griffith, M.C.; Lam, N.; Wilson, J. Displacement-Based Seismic Analysis for out-of-Plane Bending of Unreinforced Masonry Walls. *Earthq. Eng. Struct. Dyn.* **2002**, *31*, 833–850.
41. Sarhosis, V.; Milani, G.; Formisano, A.; Fabbrocino, F. Evaluation of different approaches for the estimation of the seismic vulnerability of masonry towers. *Bull. Earthq. Eng.* **2018**, *16*, 1511–1545, doi:10.1007/s10518-017-0258-8.
42. Mallardo, V.; Malvezzi, R.; Milani, E.; Milani, G. Seismic vulnerability of historical masonry buildings: A case study in Ferrara. *Eng. Struct.* **2008**, *30*, 2223–2241, doi:10.1016/j.engstruct.2007.11.006.
43. Kouris, E.-G. Dynamic Characteristics and Rocking Response of a Byzantine Medieval Tower. *J. Civ. Eng. Sci.* **2017**, *6*, 14–23, doi:10.5963/JCES0601002.
44. Makris, N.; Alexakis, H. Limit equilibrium analysis of masonry buttresses and towers under lateral and gravity loads. *Arch. Appl. Mech.* **2015**, *85*, 1915–1940, doi:10.1007/s00419-015-1027-2.
45. Saisi, A.; Gentile, C. Investigation Strategy for Structural Assessment of Historic Towers. *Infrastructures* **2020**, *5*, 106, doi:10.3390/infrastructures5120106.
46. Chrysostomou, C.; Kyriakides, N.; Kappos, A.; Kouris, L.; Georgiou, E.; Millis, M. Seismic Retrofitting and Health Monitoring of School Buildings of Cyprus. *Open Constr. Build. Technol. J.* **2013**, *7*, 208–220, doi:10.2174/1874836801307010208.
47. Ubertini, F.; Comanducci, G.; Cavalagli, N. Vibration-based structural health monitoring of a historic bell-tower using output-only measurements and multivariate statistical analysis. *Struct. Health Monit.* **2016**, *15*, 438–457, doi:10.1177/1475921716643948.
48. Chrysostomou, C.Z.; Kyriakides, N.; Kappos, A.J.; Kouris, L.; Papanikolaou, V.; Dimitrakopoulos, E.G.; Giouvanidis, A.I.; Georgiou, E. Seismic Safety and Vulnerability Mitigation of School Buildings. In Proceedings of the 4th International fib Congress 2014: Improving Performance of Concrete Structures, FIB 2014, Mumbai, India, 10–13 February 2014; pp. 122–124.
49. Kouris, L.A.S.L.; Penna, A.; Magenes, G. Damage detection of an unreinforced stone masonry two storeys building based on damping estimate. In *Brick and Block Masonry*; CRC Press: Boca Raton, FL, USA, 2016; pp. 2425–2432. ISBN 978-1-138-02999-6.
50. Kouris, L.A.S.; Penna, A.; Magenes, G. Seismic damage diagnosis of a masonry building using short-term damping measurements. *J. Sound Vib.* **2017**, *394*, 366–391, doi:10.1016/j.jsv.2017.02.001.
51. Kouris, L.A.S.; Penna, A.; Magenes, G. Dynamic Modification and Damage Propagation of a Two-Storey Full-Scale Masonry Building. *Adv. Civ. Eng.* **2019**, *2019*, 1–21, doi:10.1155/2019/2396452.
52. Gentile, C.; Saisi, A. Ambient vibration testing of historic masonry towers for structural identification and damage assessment. *Constr. Build. Mater.* **2007**, *21*, 1311–1321, doi:10.1016/j.conbuildmat.2006.01.007.
53. Stanko, D.; Markušić, S.; Strelec, S.; Gazdek, M. Seismic response and vulnerability of historical Trakošćan Castle, Croatia using HVSR method. *Env. . Earth Sci.* **2016**, *75*, 1–14, doi:10.1007/s12665-015-5185-x.
54. Standoli, G.; Giordano, E.; Milani, G.; Clementi, F. Model Updating of Historical Belfries Based on Oma Identification Techniques. *Int. J. Arch. Herit.* **2020**, 1–25, doi:10.1080/15583058.2020.1723735.
55. Bru, D.; Ivorra, S.; Betti, M.; Adam, J.M.; Bartoli, G. Parametric dynamic interaction assessment between bells and supporting slender masonry tower. *Mech. Syst. Signal Process.* **2019**, *129*, 235–249, doi:10.1016/j.ymssp.2019.04.038.
56. Stober, D.; Žarnić, R.; Penava, D.; Podmanicki, M.T.; Virgej-Đurašević, R. Application of HBIM as a Research Tool for Historical Building Assessment. *Civ. Eng. J.* **2018**, *4*, 1565, doi:10.28991/cej-0309195.
57. KEDAK. *The Towers of Mount Athos*; Konstantinou, M., Nicodimos, L., Papangellos, I., Moustakas, S., Eds.; Ministry of Macedonia-Thrace, Centre for preservation of Mount Athos Heritage: Thessaloniki, Greece, 2002; ISBN 960-859-67-7-7.
58. Munteanu, P.B. The Archaeology of the Medieval Towers in Mount Athos. An Attempt of Archaeological Research. *Rev. Transilv.* **2017**, 65–67, Available online: http://digital-library.ulbsibiu.ro/jspui/bitstream/123456789/1981/15/12%20-%20Muntean%20Besliu%20Petre%20-%20The%20archaeology%20of%20the%20medieval%20towers%20in%20Mount%20Athos.pdf; (accessed date: 15/04/2018).
59. Torelli, G.; D'Ayala, D.; Betti, M.; Bartoli, G. Analytical and numerical seismic assessment of heritage masonry towers. *Bull. Earthq. Eng.* **2020**, *18*, 969–1008, doi:10.1007/s10518-019-00732-y.
60. Milani, G. Fast Vulnerability Evaluation of Masonry Towers by Means of an Interactive and Adaptive 3D Kinematic Limit Analysis with Pre-assigned Failure Mechanisms. *Int. J. Arch. Herit.* **2019**, *13*, 941–962, doi:10.1080/15583058.2019.1645241.
61. Liakos, D. The Byzantine bell-tower in Vatopedi Monastery on Mount Athos (1427). The Sculpted decoration and its significance (with 24 figures). *Jahrb. Der Osterr. Byz.* **2016**, *1*, 153–168, doi:10.1553/joeb65s153.
62. Kouris, E.G. Recent Methodologies for Estimating Traditional Structures. Ph.D. Thesis, Aristotle Univeristy of Thessaloniki, Thessaloniki, Greece, 2019.
63. Penava, D.; Kraus, I.; Petronijević, M.; Schmid, G. Dynamic Soil-Structure Analysis of Tower-Like Structures Using Spectral Elements. *Teh. Vjesn. Tech. Gaz.* **2018**, *25*, 738–747, doi:10.17559/tv-20160302114117.
64. Lagomarsino, S.; Calderini, C. The dynamical identification of the tensile force in ancient tie-rods. *Eng. Struct.* **2005**, *27*, 846–856, doi:10.1016/j.engstruct.2005.01.008.
65. Milani, G.; Lourenço, P.; Tralli, A. 3D homogenized limit analysis of masonry buildings under horizontal loads. *Eng. Struct.* **2007**, *29*, 3134–3148, doi:10.1016/j.engstruct.2007.03.003.

66. Ramos, L.F.; Marques, L.; Lourenço, P.B.; De Roeck, G.; Campos-Costa, A.; Roque, J.C.A. Monitoring historical masonry structures with operational modal analysis: Two case studies. *Mech. Syst. Signal Process.* **2010**, *24*, 1291–1305, doi:10.1016/j.ymssp.2010.01.011.
67. Kappos, A.J.; Penelis, G.G.; Drakopoulos, C.G. Evaluation of Simplified Models for Lateral Load Analysis of Unreinforced Masonry Buildings. *J. Struct. Eng.* **2002**, *128*, 890–897, doi:10.1061/(asce)0733-9445(2002)128:7(890).
68. Quinn, N.; D'Ayala, D. Assessment of the Realistic Stiffness and Capacity of the Connections in Quincha Frames to Develop Numerical Models. In Proceedings of the 2nd International Conference on Structural Health Assessment of Timber Structures, SHATIS 2013, Trento, Italy, 4–6 September 2013; Volume 778, pp. 526–533.
69. Kouris, L.A.S.; Bournas, D.A.; Akintayo, O.T.; Konstantinidis, A.A.; Aifantis, E.C. A gradient elastic homogenisation model for brick masonry. *Eng. Struct.* **2020**, *208*, 110311, doi:10.1016/j.engstruct.2020.110311.
70. Hendry, A.W. *Structural Masonry*; Macmillan Press: London, UK, 1998.
71. Bartoli, G.; Betti, M.; Giordano, S. In situ static and dynamic investigations on the "Torre Grossa" masonry tower. *Eng. Struct.* **2013**, *52*, 718–733, doi:10.1016/j.engstruct.2013.01.030.
72. Boschi, S.; Galano, L.; Vignoli, A. Mechanical characterisation of Tuscany masonry typologies by in situ tests. *Bull. Earthq. Eng.* **2019**, *17*, 413–438, doi:10.1007/s10518-018-0451-4.
73. Moropoulou, A.; Cakmak, A.; Lohvyn, N. Earthquake resistant construction techniques and materials on Byzantine monuments in Kiev. *Soil Dyn. Earthq. Eng.* **2000**, *19*, 603–615, doi:10.1016/s0267-7261(00)00021-x.
74. Çakmak, A.; Moropoulou, A.; Mullen, C. Interdisciplinary study of dynamic behavior and earthquake response of Hagia Sophia. *Soil Dyn. Earthq. Eng.* **1995**, *14*, 125–133, doi:10.1016/0267-7261(94)00031-b.
75. CEN. *Eurocode 5: Design of Timber Structures. EN 1995*; European Committee for Standardization: Brussels, Belgium, 2004.
76. Saisi, A.; Gentile, C.; Guidobaldi, M. Post-earthquake continuous dynamic monitoring of the Gabbia Tower in Mantua, Italy. *Constr. Build. Mater.* **2015**, *81*, 101–112, doi:10.1016/j.conbuildmat.2015.02.010.
77. Saisi, A.; Guidobaldi, M.; Gentile, C. On Site Investigation and Continuous Dynamic Monitoring of a Historic Tower in Mantua, Italy. In Proceedings of the 6th International Conference on Emerging Technologies in Nondestructive Testing(ETNDT6), Brussels, Belgium, 27–29 May 2015.
78. Bayraktar, A.; Türker, T.; Sevım, B.; Altunişik, A.C.; Yildirim, F. Modal Parameter Identification of Hagia Sophia Bell-Tower via Ambient Vibration Test. *J. Nondestruct. Eval.* **2009**, *28*, 37–47, doi:10.1007/s10921-009-0045-9.
79. Russo, G.; Bergamo, O.; Damiani, L.; Lugato, D. Experimental analysis of the "Saint Andrea" Masonry Bell Tower in Venice. A new method for the determination of "Tower Global Young's Modulus E." *Eng. Struct.* **2010**, *32*, 353–360, doi:10.1016/j.engstruct.2009.08.002.
80. Ivorra, S.; Palomo, M.J.; Verdu, G.; Zasso, A. Dynamic Forces Produced by Swinging Bells. *Meccanica* **2006**, *41*, 47–62, doi:10.1007/s11012-005-7973-y.
81. DiTommaso, R.; Mucciarelli, M.; Parolai, S.; Picozzi, M. Monitoring the structural dynamic response of a masonry tower: Comparing classical and time-frequency analyses. *Bull. Earthq. Eng.* **2012**, *10*, 1221–1235, doi:10.1007/s10518-012-9347-x.
82. Diaferio, M.; Foti, D.; Giannoccaro, N.I. Modal Parameters Identification on Environmental Tests of an Ancient Tower and Validation of Its FE Model. *Int. J. Mech.* **2016**, *10*, 80–89.
83. Aloisio, A.; Capanna, I.; Cirella, R.; Alaggio, R.; Di Fabio, F.; Fragiacomo, M. Identification and Model Update of the Dynamic Properties of the San Silvestro Belfry in L'Aquila and Estimation of Bell's Dynamic Actions. *Appl. Sci.* **2020**, *10*, 4289, doi:10.3390/app10124289.
84. Bartoli, G.; Betti, M.; Vignoli, A. A numerical study on seismic risk assessment of historic masonry towers: A case study in San Gimignano. *Bull. Earthq. Eng.* **2016**, *14*, 1475–1518, doi:10.1007/s10518-016-9892-9.
85. Preciado, A.; Budelmann, H.; Bartoli, G. Earthquake Protection of Colonial Bell Towers in Colima, Mexico with Externally Prestressed FRPs. *Int. J. Arch. Herit.* **2016**, *10*, 499–515, doi:10.1080/15583058.2014.1003624.
86. Bassoli, E.; Vincenzi, L.; Bovo, M.; Mazzotti, C. Dynamic Identification of an Ancient Masonry Bell Tower Using a MEMS-Based Acquisition System. In Proceedings of the 2015 IEEE Workshop on Environmental, Energy, and Structural Monitoring Systems (EESMS) Proceedings; IEEE, Trento, Italy, 9–10 July 2015; pp. 226–231.
87. Ceroni, F.; Pecce, M.; Manfredi, G. Seismic Assessment of the Bell Tower of Santa Maria Del Carmine: Problems and Solutions. *J. Earthq. Eng.* **2009**, *14*, 30–56, doi:10.1080/13632460902988968.
88. Gentile, C.; Saisi, A.; Cabboi, A. Structural Identification of a Masonry Tower Based on Operational Modal Analysis. *Int. J. Arch. Herit.* **2014**, *9*, 98–110, doi:10.1080/15583058.2014.951792.
89. Saisi, A.; Gentile, C.; Ruccolo, A. Pre-diagnostic prompt investigation and static monitoring of a historic bell-tower. *Constr. Build. Mater.* **2016**, *122*, 833–844, doi:10.1016/j.conbuildmat.2016.04.016.
90. Saisi, A.; Guidobaldi, M.; Gentile, C. On Site Investigation and Health Monitoring of a Historic Tower in Mantua, Italy. *Appl. Sci.* **2016**, *6*, 173, doi:10.3390/app6060173.
91. Pieraccini, M.; Dei, D.; Mecatti, D.; Parrini, F. Dynamic Testing of Historic Towers Using an Interferometric Radar from an Unstable Measurement Position. *J. Nondestruct. Eval.* **2013**, *32*, 398–404, doi:10.1007/s10921-013-0193-9.
92. Bartoli, G.; Betti, M.; Marra, A.M.; Monchetti, S. Semiempirical Formulations for Estimating the Main Frequency of Slender Masonry Towers. *J. Perform. Constr. Facil.* **2017**, *31*, 04017025, doi:10.1061/(asce)cf.1943-5509.0001017.
93. Lagomarsino, S.; Podestà, S.; Resemini, S. Seismic Response of Historical Churches. In Proceedings of the 12th European Conference on Earthquake Engineering; London, UK, 9–13 September 2002; p. 123.

94. Kárník, V.; Procházková, D.; Schenková, Z.; Ruprechtová, L.; Dudek, A.; Drimmel, J.; Schmedes, E.; Leydecker, G.; Rothe, J.P.; Guterch, B.; et al. Map of isoseismals of the main Friuli earthquake of 6 May 1976. *Pure Appl. Geophys. Pageoph* **1978**, *116*, 1307–1313, doi:10.1007/bf00874689.
95. Bindi, D.; Pacor, F.; Luzi, L.; Massa, M.; Ameri, G. The Mw 6.3, 2009 L'Aquila Earthquake: Source, Path and Site Effects from Spectral Analysis of Strong Motion Data. *Geophys. J. Int.* **2009**, *179*, 1573–1157.
96. Decanini, L.; De Sortis, A.; Goretti, A.; Langenbach, R.; Mollaioli, F.; Rasulo, A. Performance of Masonry Buildings during the 2002 Molise, Italy, Earthquake. *Earthq. Spectra* **2004**, *20*, 191–220, doi:10.1193/1.1765106.
97. Abrams, D.P.; Angel, R.; Uzarski, J. Out-of-Plane Strength of Unreinforced Masonry Infill Panels. *Earthq. Spectra* **1996**, *12*, 825–844, doi:10.1193/1.1585912.
98. Ewing, R.D.; Kariotis, J.C. Methodology for Mitigation of Seismic Hazards in Existing Unreinforced Masonry Buildings: Wall Testing, Out-of-Plane. Topical Report 04. 1981. Available online: https://nehrpsearch.nist.gov/static/files/NSF/PB83125005.pdf (accessed date: 15/03/2018).
99. Lagomarsino, S. On the vulnerability assessment of monumental buildings. *Bull. Earthq. Eng.* **2006**, *4*, 445–463, doi:10.1007/s10518-006-9025-y.
100. Griffith, M.C.; Magenes, G.; Melis, G.; Picchi, L. Evaluation of Out-of-Plane Stability of Unreinforced Masonry Walls Subjected to Seismic Excitation. *J. Earthq. Eng.* **2003**, *7*, 141–169, doi:10.1080/13632460309350476.
101. Fajfar, P. Capacity Spectrum Method Based on Inelastic Demand Spectra. *Earthq. Eng. Struct. Dyn.* **1999**, *28*, 979–994.
102. Fajfar, P. A Nonlinear Analysis Method for Performance-Based Seismic Design. *Earthq. Spectra* **2000**, *16*, 573–592, doi:10.1193/1.1586128.
103. European Committee for Standardization. *Eurocode 6: Design of Masonry Structures; Part 1: General Rules for Buildings*; CEN: Brussels, Belgium, 2004; Volume 1.
104. Fonti, R.; Borri, A.; Barthel, R.; Candela, M.; Formisano, A. Rubble Masonry Response under Cyclic Actions: Experimental Tests and Theoretical Models. *Int. J. Mason. Res. Innov.* **2017**, *2*, doi:10.1504/IJMRI.2017.10003258.
105. Formisano, A. Seismic Behaviour and Retrofitting of the Poggio Picenze Historical Centre Damaged by the L'Aquila Earthquake. In *Proceedings of the 11th International Conference on Computational Structures Technology*; Topping, B.H.V., Ed.; Civil-Comp Press: Stirlingshire, Scotland, 2012; p. 199.
106. Curti, E.; Podestà, S.; Scandolo, L. Simplified Mechanical Model for the Seismic Vulnerability Evaluation of Belfries. *Int. J. Arch. Herit.* **2012**, *6*, 605–625, doi:10.1080/15583058.2011.594932.
107. Vukobratović, V.; Fajfar, P. A method for the direct determination of approximate floor response spectra for SDOF inelastic structures. *Bull. Earthq. Eng.* **2015**, *13*, 1405–1424, doi:10.1007/s10518-014-9667-0.
108. Politopoulos, I.; Feau, C. Some aspects of floor spectra of 1DOF nonlinear primary structures. *Earthq. Eng. Struct. Dyn.* **2007**, *36*, 975–993, doi:10.1002/eqe.664.
109. European Committee for Standardization. *Eurocode 8, Design of Structures for Earthquake Resistance. Part 1: General Rules, Seismic Actions and Rules for Buildings*. *Eur. Stand. NF EN*; CEN: Brussels, Belgium, 1998; Volume 1.
110. Bommer, J.J.; Elnashai, A.S. Displacement Spectra for Seismic Design. *J. Earthq. Eng.* **1999**, *3*, 1–32, doi:10.1080/13632469909350338.
111. Faccioli, E.; Paolucci, R.; Rey, J. Displacement Spectra for Long Periods. *Earthq. Spectra* **2004**, *20*, 347–376, doi:10.1193/1.1707022.
112. Tsapanos, T.M. *Seismicity and Seismic Hazard Assessment in Greece*; Springer: Dordrecht, The Netherlands, 2008; pp. 253–270.
113. Kassaras, I.; Kapetanidis, V.; Ganas, A.; Tzanis, A.; Kosma, C.; Karakonstantis, A.; Valkaniotis, S.; Chailas, S.; Kouskouna, V.; Papadimitriou, P. The New Seismotectonic Atlas of Greece (v1.0) and Its Implementation. *Geosciences* **2020**, *10*, 447, doi:10.3390/geosciences10110447.
114. Whitman, R.V.; Anagnos, T.; Kircher, C.A.; Lagorio, H.J.; Lawson, R.S.; Schneider, P. Development of a National Earthquake Loss Estimation Methodology. *Earthq. Spectra* **1997**, *13*, 643–661, doi:10.1193/1.1585973.
115. Kouris, L.A.S.; Kappos, A.J. Fragility Curves and Loss Estimation for Traditional Timber-Framed Masonry Buildings in Lefkas, Greece. In *Seismic Assessment, Behavior and Retrofit of Heritage Buildings and Monuments*; Springer: Dordrecht, The Netherland, 2015; Volume 37, pp. 199–233.
116. Formisano, A.; Marzo, A. Simplified and refined methods for seismic vulnerability assessment and retrofitting of an Italian cultural heritage masonry building. *Comput. Struct.* **2017**, *180*, 13–26, doi:10.1016/j.compstruc.2016.07.005.
117. Kouris, L.A.S.; Kappos, A.J. Derivation of Fragility Curves for Traditional Timber-Framed Masonry Buildings Using Nonlinear Static Analysis. In Proceedings of the 4th ECCOMAS Thematic Conference on Computational Methods in Structural Dynamics and Earthquake Engineering, Kos Island, Greece, 12–14 June 2013; pp. 1339–1348.
118. Kouris, L.A.S. Seismic fragility curves for timber-framed masonry structures based on empirical damage data. *Int. J. Sustain. Mater. Struct. Syst.* **2016**, *2*, 233, doi:10.1504/IJSMSS.2016.078715.
119. Federal Emergency Management Agency. *HAZUS: Multi-Hazard Loss Estimation Methodology TECHNICAL and USER'S MANUAL*; FEMA: Washington, DC, USA, 2003.